11 Jan 2018

Seismic Performance of Hollow-Core HC-FCS Columns having Inner Steel Tube with High Diameter to Thickness Ratio

Mohanad M. Abdulazeez

Mohamed ElGawady
Missouri University of Science and Technology, elgawadym@mst.edu

SEISMIC PERFORMANCE OF HOLLOW-CORE HC-FCS COLUMNS HAVING INNER STEEL TUBE WITH HIGH DIAMETER TO THICKNESS RATIO

Mohanad M. Abdulazeez
Graduate Research Assistant and PhD student
Department of Civil, Architectural and Environmental Engineering
Missouri University of Science and Technology
1401 N. Pine Street, 212 Butler-Carlton Hall, Rolla, MO 65409
Tel: 573-202-9988; Email: mma548@mst.edu

Mohamed A. ElGawady, Corresponding Author
Benavides Associate Professor
Department of Civil, Architectural & Environmental Engineering
Missouri University of Science and Technology
1401 N. Pine Street, 324 Butler-Carlton Hall, Rolla, MO 65409
Tel: 573-341-6947; Fax: 573-341-4729; Email: elgawadym@mst.edu

Word count: 3,046 words text + 11 tables/figures x 250 words (each) = 5,796 words

Submission Date: August 1st, 2017

ABSTRACT
This paper experimentally investigates the seismic behavior of a large-scale hollow-core fiber-reinforced polymer-concrete-steel HC-FCS column under seismic cyclic loading. The HC-FCS column consisted of a concrete shell sandwiched between an outer fiber-reinforced polymer (FRP) tube and an inner steel tube. The FRP tube provides continuous confinement for the concrete shell along the height of the column while the steel tube provides the required flexural strength. The tested column has an inner steel tube that had a diameter-to-thickness ratio (D_i/t) of 254. The seismic performance of the precast HC-FCS column was compared to that of HC-FCS column having (D_i/t) of 64. Three-dimensional numerical models were also developed using LS_DYNA software for modeling the HC-FCS columns. This study revealed that HC-FCS columns having very high (D_i/t) and short embedded lengths do not dissipate high levels of energy and display nonlinear elastic performance due to steel tube slippage. However, the use of small values of (D_i/t) combined with generous embedment length results in a nonlinear inelastic behavior, high energy dissipation, and ductile behavior.

INTRODUCTION
The National Bridge Inventory (FHWA 2013) classified 63,522 bridges as "structurally deficient" and 84,348 bridges as "functionally obsolete" with many of them needing to be repaired, rehabilitated, or replaced. Therefore, a rapid construction method to address this challenge is required.

Accelerated bridge construction (ABC) reduces traffic disruptions and life-cycle costs and improves construction quality and safety, resulting in more sustainable development [1]. The use of precast concrete bridge elements is one strategy that can reduce on-site construction time, field labor requirements and traffic impact.

Recently, interest has been growing in the use of fiber reinforced polymer (FRP) tubes in construction as a replacement for the outer steel tube of double skin tubular (DSTCs) columns [2, 3]. The proposed column, hollow core FRP-Concrete-Steel (HC-FCS), consists of an inner steel tube and an outer FRP tube, with a concrete shell placed in-between the two tubes (Fig. 1). HC-FCS composite columns have several advantages as a precast element over conventional reinforced concrete or structural steel. The concrete infill is confined by both FRP and steel tubes, which results in a triaxial state of compression that increases the strength and strain capacity of the concrete infill and enhances the seismic performance [5-8]. The concrete shell reduces the susceptibility of the steel tube to local and global buckling.

The main objective of this study is to investigate the performance of HC-FCS column under axial and quasi-static cyclic loads. The column had a steel tube diameter-to-thickness ratio (D_i/t) of 254. The results of this column were compared to those of another HC-FCS column having Di/t of 64 [10].

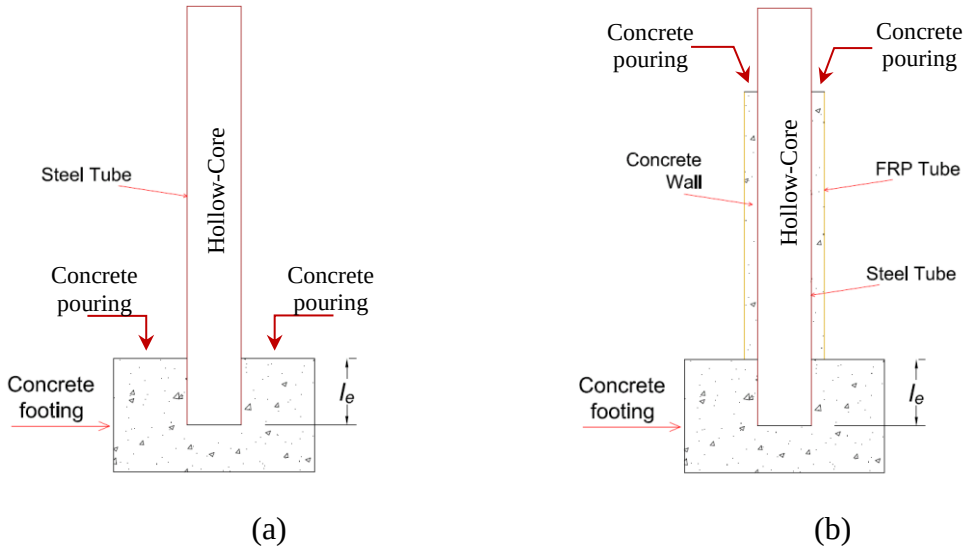

(a) (b)

FIGURE 1 General arrangement of the construction of the HC-FCS column (a) inserting the steel tube and casting the footing, (b) installing the FRP tube and pouring the concrete shell.

EXPERIMENTAL PROGRAM

In this study, a 0.4-scale HC-FCS column, F4-24-E3-0.5-4 was tested under constant axial load and lateral cyclic load. The F4-24-E3(0.5)4 column had a circular cross section with an outer diameter (D_f) of 24 inches and a clear height of 80 inches. The lateral load was applied at a height of 95 inches with a shear span-to-depth ratio of approximately 4.0.

The column consisted of an outer filament-wound GFRP tube with a thickness of 0.38 inches. The inner steel tube had an outer diameter of 16 inches and a thickness of 0.063 inches corresponding to inner-diameter-to-thickness D_i/t_s of 254. The steel tube was manufactured in the High-bay Structural Engineering Research Laboratory at Missouri University of Science and Technology by performing a seam-welding (full-penetration groove weld according to AWS 2000) for a 0.063-inches steel sheet cut and rolled to the required dimensions (length x circumference) prior to the welding. A concrete shell with a thickness of 4 inches was sandwiched between the steel and FRP tubes (Fig. 2).

The columns' label used in the current experimental work consisted of four segments. The first segment is a letter "F" in reference to flexural testing, followed by the column's height-to-outer diameter ratio (H/D_f). The second segment refers to the column's outer diameter (D_f) in inches. The third segment refers to the GFRP matrix using "E" for epoxy base matrices; this is followed by the GFRP thickness in 1/8 inch, steel thickness in 1/8 inch, and concrete shell thickness in inches.

The steel tube of the column was embedded into the footing while the FRP tube truncated at the face of the footing without any embedment. The embedment depth, l_e, was determined using equation 1 [9]

$$\frac{D_i t_s F_u}{\left(l_e{}^2\right)} \leq 3.3\sqrt{f'_{c,FT}} \quad (1)$$

where D_i is the steel tube outer diameter (being 16 inches), t_s is the steel tube thickness (being 0.063 inches), and F_u is the ultimate stress of steel tube (being 56,000 psi), and $f'_{c,FT}$ is the unconfined cylindrical compressive strength of the concrete footing (being 5,500 psi). Using these values, an embedded length of 20 inches was deduced. Therefore, during the experimental work, l_e of 20 inches corresponding to 1.25 D_i (D_i is the inner diameter of the steel tube) was used to achieve the full embedment of the HC-FCS column (Fig. 1).

The concrete footing that was used in this study had a length x width x depth of 60 inches x 48 inches x 34 inches with bottom reinforcements of 7-#7, top reinforcements of 6-#7, and shear reinforcement of #4 at 2.5 inches (Fig. 2). The steel cage of the footing was installed into the formwork.

The construction steps were as follows: 1) preparing and installing the reinforcement cages of the footings; 2) installing the steel tube into the footing cage with an embedded length of 20 inches; 3) pouring the concrete of the footing; 4) installing the GFRP tube and pouring the concrete of the concrete shell; 5) installing the reinforcement cage of the column head with dimensions of length x width x depth of 30 inches x 30 inches x 32 inches around the and concrete pouring.

The used GFRP tube, based on the manufacturer's datasheet, had elastic modulus of 677 ksi, hoop elastic modulus of 3,020 ksi, axial ultimate stress of 12,150 psi, and hoop rupture stress of 40,150 psi.

For column F4-24-E3(0.5)4, the steel tube had yield stress of 56,000 psi, ultimate stress of 63,000 psi, yielded strain of 2.35%, and an ultimate strain of 6.7%. For column F4-24-E324, the steel tube had yield stress of 42,000 psi, ultimate stress of 58,000 psi, yielded strain of 2.35%, and an ultimate strain of 23%. The steel rebar had yield stress of 60,000 (psi), ultimate stress of 90,000 (psi), and ultimate strain of 0.08. The rebar properties are based on the manufacturer's data sheet while the steel tube properties were determined through tensile steel-coupon testing according to ASTM A1067.

Pea gravel with a maximum aggregate size of 3/8 inches was used for concrete mixtures. The unconfined concrete strengths ($f'c$) for F4-24-E324 [15] at 28 days and at the day of the test were 4,790 (psi) and 5,222 (psi) for the column, while 5,360 (psi) and 5,660 (psi) were obtained for the footing at the same ages, respectively. The unconfined concrete strength for F4-24-E3(0.5)4 at 28 days and at the day of the test were 6,305 (psi) and 6,610 (psi) for the column, while 5,960 (psi) and 6,445 (psi) were obtained for the footing of the same age, respectively.

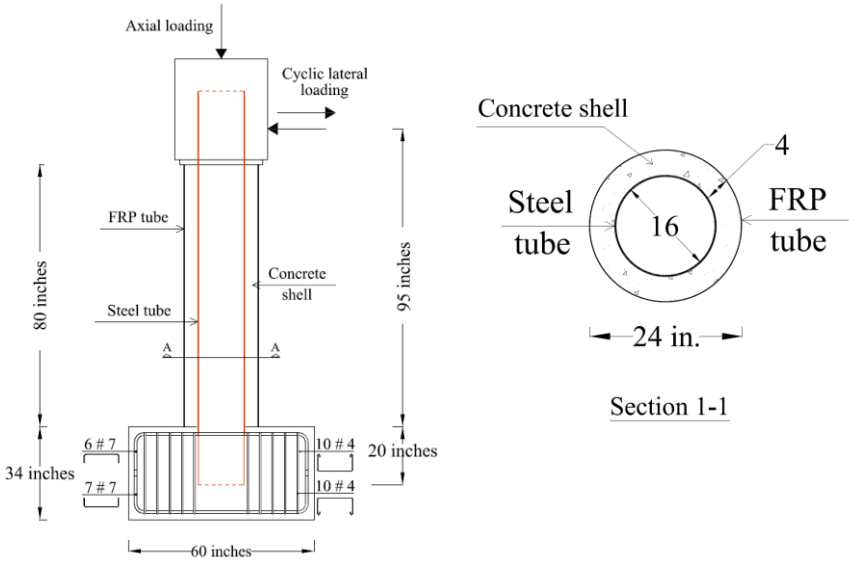

(a) (b)

FIGURE 2 construction layout of the column (a) elevation, (b) column cross-section.

EXPERIMENTAL WORK AND INSTRUMENTATIONS

Sixteen linear variable displacement transducers (LVDTs) and string potentiometers (SPs) were assigned for measuring different displacements in each test specimen [Figure 3 (a)]. Four LVDTs were mounted on each of the north and south faces of the column to measure the vertical displacements along the potential plastic hinge region. Two more LVDTs were attached to the footing for measuring the uplift and sliding of the footing during the test. The effects of the footing uplift and sliding were considered before calculating the lateral displacement and curvature of the column.

Forty strain gauges were installed on the FRP tube at five levels with 5 inch spacing between them. Four horizontal and four vertical strain gauges were installed at each level [Figure 3 (b)]. Sixty-four strain gauges were installed inside the steel tube at seven levels with a spacing of 5 inches [Fig. 3 (c)]. Four horizontal and four vertical strain gauges were installed at each level. A high definition webcam was placed inside the steel tube 20 inches from the top of the footing level to film any potential buckling of the steel tube and any internal damage.

Three embedded strain gauges were used to measure the internal stresses of the concrete shell. The sensor dimensions are 1.2-inch x 0.39-inch x 0.12 inches sensing grid with an effective gauge length of 0.6 inches. The gauge is waterproof and it is designed to have a treated surface with a honeycomb pattern that enables an adequate bond to concrete. The sensor consists of a 0.6 inches 120 ohm (Ω) foil strain gage (copper-nickel alloy on acrylate material base). The strain gauges were mounted in the three (x, y, and z) direction inside the concrete shell by attaching them temporarily on a plastic frame at 4 inches height from the top footing level on the south side of the column (Fig.4).

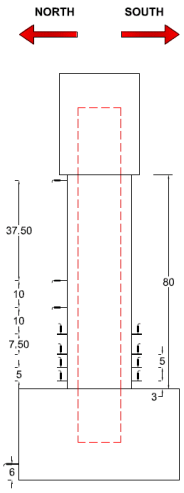

(a)

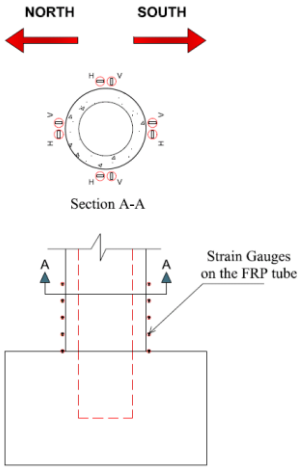

(b)

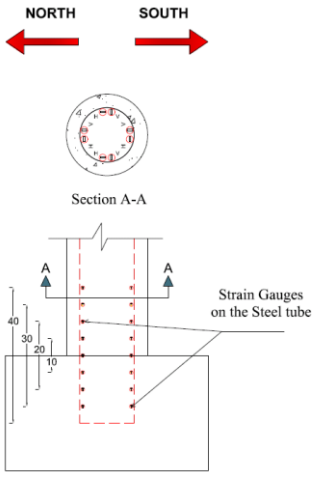

(c)

FIGURE 3 Strain gauges layout: (a) LVDT's and SP's installed, (b) mounted on GFRP tube, (c) mounted on steel tube.

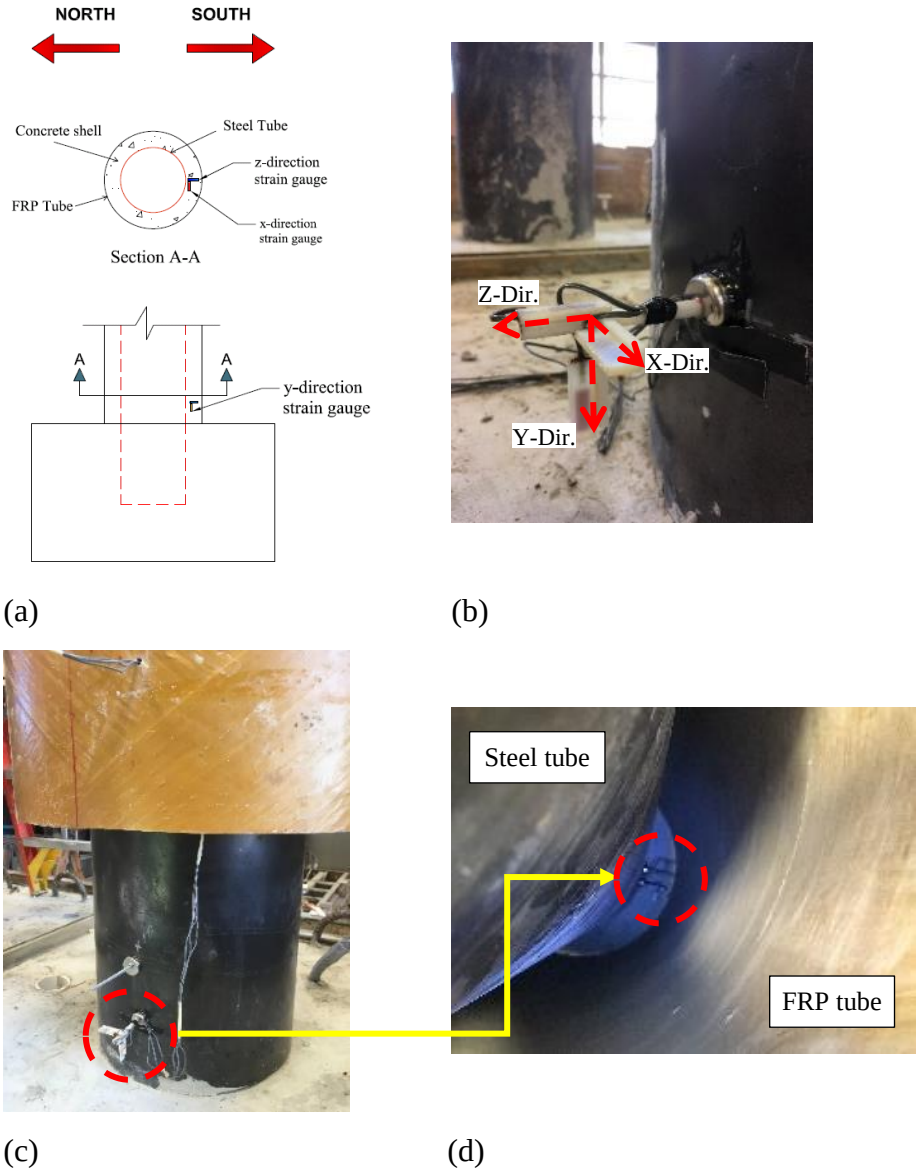

(a) (b)

(c) (d)

FIGURE 4 Embedded strain gauges into the concrete shell (a) layout, (b) mounted on the plastic frame that temporarily attached to the steel tube on the south side, (c) setting down the GFRP tube, (d) the embedded strain gauges final location before pouring the concrete shell.

LOADING PROTOCOL AND TEST SETUP

Constant axial load, P, of 110 kips corresponding to 5% of the axial load capacity of the equivalent RC-column, P_o, with the same diameter and 1% longitudinal reinforcement ratio was applied to the column using six external prestressing strands (Fig. 5). The P_o was calculated using Eq. 2 (AASHTO-LRFD 2012):

$$P_o = A_s F_y + 0.85(A_c - A_s) f'c \quad (2)$$

where A_s = the cross-sectional area of the longitudinal steel reinforcements, A_c = the cross-sectional area of the concrete column, and F_y = the yield stress of the longitudinal steel reinforcements. The prestressing strands were supported by a rigid steel beam atop the column and the column's footing. The prestressing force was applied using two servo-controlled jacks that kept the prestressing force constant during the test.

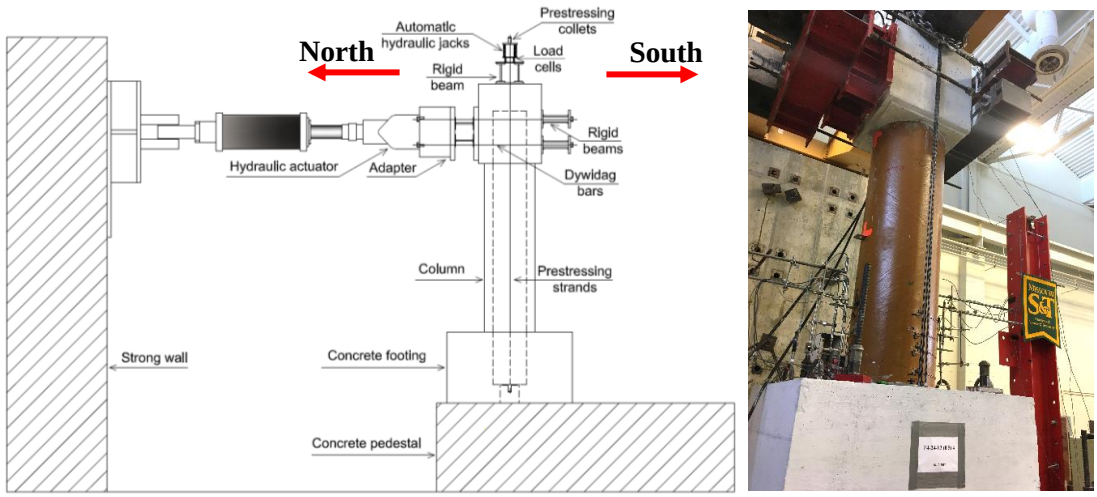

(a) (b)

FIGURE 5 (a) Layout of the test setup, (b) The F4-24-E3(0.5)4 column ready for testing.

After applying the axial load, a cyclic lateral load was applied in a displacement control mode using two hydraulic actuators connected to the column loading stub. The loading regime was based on the recommendations of FEMA 2007, where the displacement amplitude a_{i+1} of the step i+1 is 1.4 times the displacement amplitude of the proceeding step (ai). Two cycles were executed for each displacement amplitude. Figure 6 illustrates the loading regime of the cyclic lateral displacement. Each loading cycle was applied in 100 sec. corresponding to a loading rate that ranged from 0.01 inch/sec. to 0.05 inch/sec.

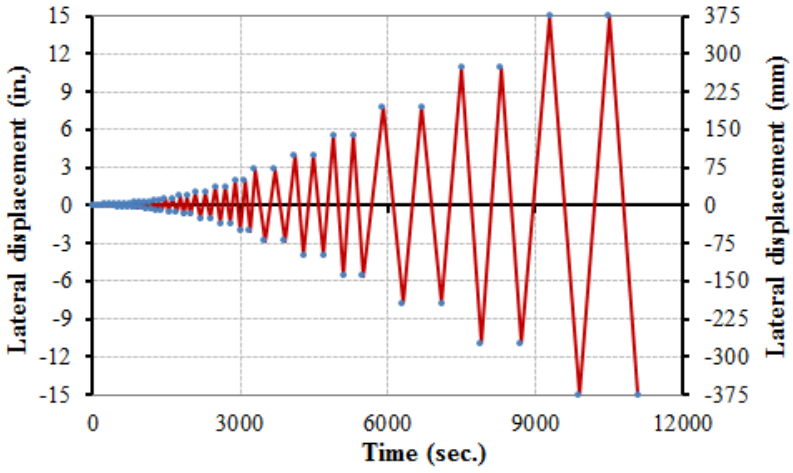

FIGURE 6 Lateral displacement loading regime.

RESULTS AND DISCUSSIONS

Generally, the embedded length and thickness of the steel tube have significant effects on the behavior of HC-FCS columns under cyclic loads [9]. The tested column in this study had a very thin steel tube that was susceptible to inward buckling instabilities, and thereby steel tube slippage led to degradation of the bending strength.

Figure 7 (a) compares the cyclic response of the two columns, F4-24-E324, and F4-24-E3(0.5)4. It is worth noting that for column F4-24-E324 [10], the steel tube thickness and embedded length into the footing were 0.25 inches (Di/t_s=64) and 25 inches corresponding to 1.6 D_i; respectively.

The lateral drift (δ) was calculated by dividing the lateral displacement measured from the actuators' displacement transducers by the shear span of 95 inches. The moment (M) at the base of the column was obtained by multiplying the force measured by the actuators' load cells by the column's height of 95 inches. The calculated moments were normalized by each steel tube cross sectional area and yield stress.

The moment capacity and the lateral drift were 237 kip.ft and 11.4% for column F4-24-E3(0.5)4, while they were 550.4 kip.ft and 14.1% for column F4-24-E324, respectively. Therefore, the normalized moment capacity and maximum lateral drift of the F4-24-E3(0.5)4 column, were 35% and 20% higher and lower than those for column F4-24-E324; respectively (Figure 7).

As shown in Figure 7, while column F4-24-E324 displayed large hysteretic loops indicating large energy dissipation, column F4-24-E3(0.5)4 displayed narrow hysteretic loops indicating low energy dissipation. Furthermore, column F4-24-E3(0.5)4 displayed approximately nonlinear elastic response due to sliding of the steel tube. To the contrary, column F4-24-E324 displayed nonlinear inelastic performance due to yielding and hardening of the steel tube. Careful examination of the video recording and comprehensive finite element modeling showed that early local buckling in the case of column F4-24-E3(0.5)4 occurred near the footing-column interface joint which gradually extended downward leading to bond deterioration between the embedded steel tube and the surrounding concrete inside the footing. As shown in Figure 8, the end section of the steel tube did not keep its circular shape. Thus, early initiation of the steel tube pull-out (slip) was observed at 2.7% lateral drift followed by bending strength dropping as shown in Figure [9 (a)].

A 3D finite element model was developed using LS_DYNA software and validated using measured response and observed damage of previous test results [7]. As shown in Figure 9 (a), the FE model was able to predict 98% of the average ultimate moment capacity of the column and 92.5% of the maximum lateral drift. In Figure 9 (b), the simulated model showed no damage into the footing which matches the test observations.

Figure 10 shows the concrete shell axial strain measured during the experimental work using the embedded strain gauge (SG) at the south (push) side and those obtained from the FE model. As shown in the figure, the FE results had a good agreement with the experimental results with high accuracy. The experimental maximum compressive

strain was 945 Microstrain at lateral drift of 5.6% compared to 910 Microstrain at 6.3% drift from the FE results.

Figure 11 illustrates the cumulative energy dissipation vs. lateral drift relation for columns F4-24-E3(0.5)4 and F4-24-E324 [10]. The energy dissipation at each lateral drift was determined as the area enclosed in the hysteretic loop of the first cycle at this drift level. The energy was calculated using the normalized normal force, i.e., the lateral force normalized by the steel tube cross sectional area and yield strength. Dissipating higher hysteretic energy reduces the seismic demand on a structure. As shown in the figure, both columns dissipated the same level of energy until drift of approximately 3.8%. Beyond that, column F4-24-E3(0.5)4 dissipated 30% less energy due to the severe local buckling followed by the steel tube slippage.

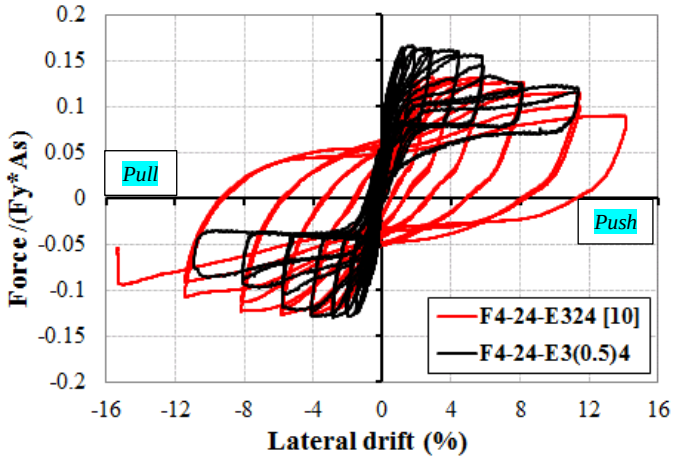

(a)

(b)

FIGURE 7 (a) Normalized moment vs. lateral drift of columns F4-24-E3(0.5)4 and F4-24-E324 [11]; (b) columns F4-24-E3(0.5)4 during the test.

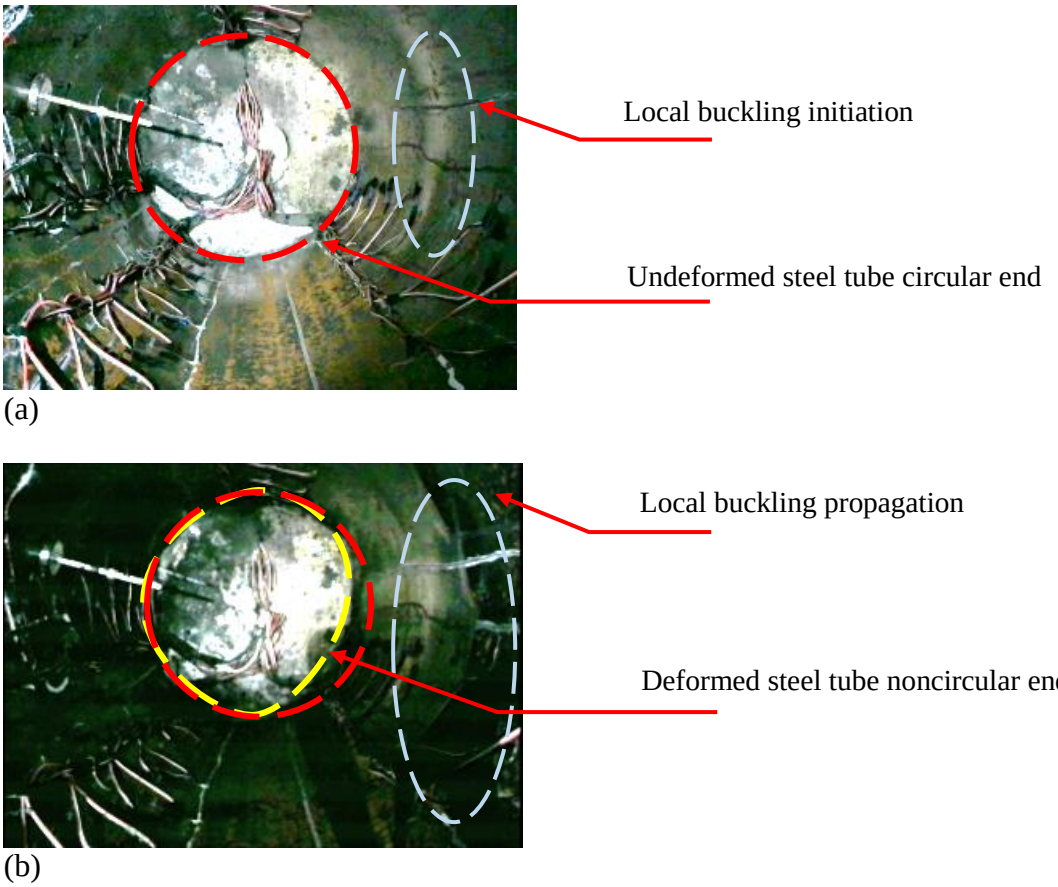

FIGURE 8 Local buckling of the steel tube of the column F4-24-E3(0.5)4 at lateral drifts of: (a) 1.4%, (b) 3.6%

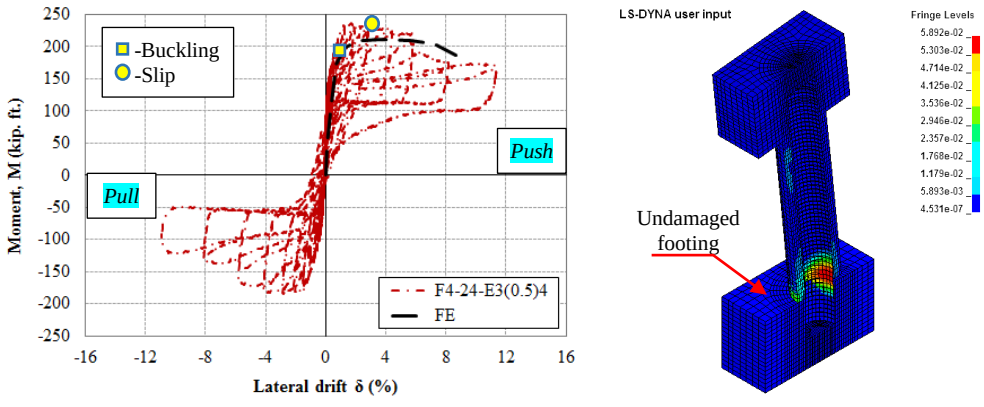

FIGURE 9 Columns F4-24-E3(0.5)4 (a) experimental vs. FE results, (b) 3D FE deformed view.

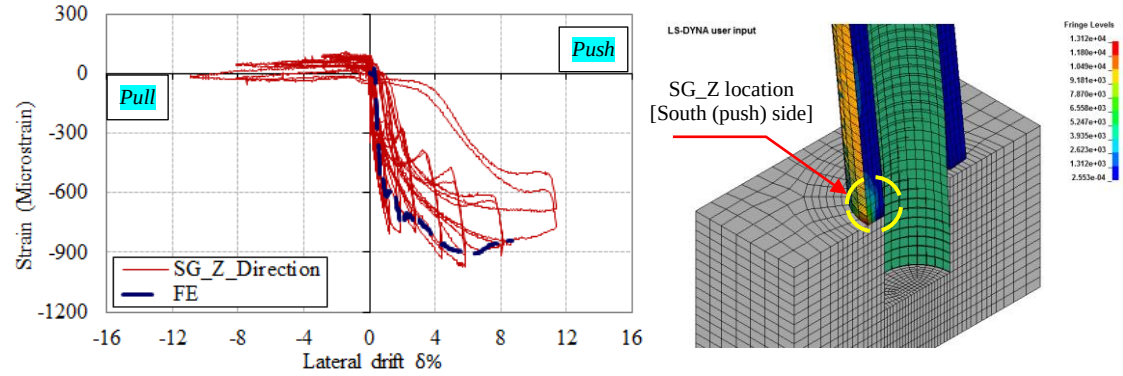

(a) (b)

FIGURE 10 Embedded train gauge (SG) of the concrete shell on the south (push) side in the z-direction (a) experimental vs. FE results, (b) 3D FE view.

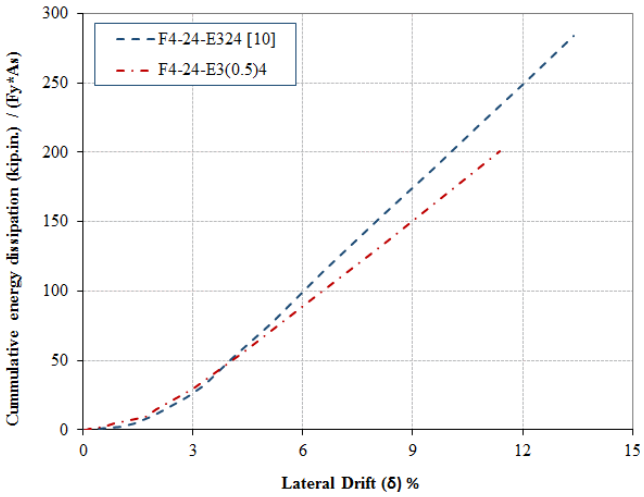

FIGURE 11 Normalized cumulative energy dissipation vs. lateral drift for columns F4-24- E3(0.5)4 and F4-24-E324 [11].

CONCLUSIONS

This paper presents the experimental results of a hollow-core fiber reinforced polymer concrete steel (HC-FCS) precast column. The HC-FCS column consists of a hollow concrete cylinder sandwiched between an outer fiber-reinforced polymer (FRP) tube and an inner steel tube. The column had an outer diameter of 24 inches, an inner steel tube diameter of 16 inches with $D_i/t_s=254$, and a height-to-diameter ratio of 4.0. The steel tube was embedded into reinforced concrete footing with an embedded length of 20 inches corresponding to 1.25 D_i, while the FRP tube acted as a formwork and provided a continuous confinement for the concrete shell and was curtailed at the top surface of the footing. The column was subjected to constant axial load and lateral cyclic load during this study and compared to the HC-FCS column that was tested by [10] under the same loading regime. The tested column in this study has a thin-walled steel tube that was early susceptible to inward buckling instabilities at small lateral drift of 1%. Therefore, steel tube slippage occurred due to the combination of the insufficient

development length and the contact debonding with the surrounding footing concrete, which led to degradation of the bending strength until the end of the test at 11.4% lateral drift.

REFERENCES

1. Dawood, H., M. Elgawady, and J. Hewes, *Factors affecting the seismic behavior of segmental precast bridge columns.* Frontiers of Structural and Civil Engineering, 2014. **8**(4): p. 388-398.
2. Teng, J. and L. Lam, *Behavior and modeling of fiber reinforced polymer-confined concrete.* Journal of Structural Engineering, 2004. **130**(11): p. 1713-1723.
3. Teng, J., et al., *Hybrid FRP–concrete–steel tubular columns: concept and behavior.* Construction and Building Materials, 2007. **21**(4): p. 846-854.
4. Zhang, B., J. Teng, and T. Yu, *Behaviour of hybrid double-skin tubular columns subjected to combined axial compression and cyclic lateral loading.* 2012.
5. Abdelkarim, O.I. and M.A. ElGawady, *Analytical and finite-element modeling of FRP-concrete-steel double-skin tubular columns.* Journal of Bridge Engineering, 2014.
6. Abdelkarim, O.I. and M.A. ElGawady, *Behavior of hollow FRP–concrete–steel columns under static cyclic axial compressive loading.* Engineering Structures, 2016. **123**: p. 77-88.
7. Abdulazeez, M.M., et al., *Effects of Footing Connections of Precast Hollow-Core Composite Columns.* 2017.
8. Abdelkarim, O.I. and M.A. ElGawady, *Concrete-filled-large deformable FRP tubular columns under axial compressive loading.* Fibers, 2015. **3**(4): p. 432-449.
9. Abdelkarim, O.I., et al., *Seismic performance of innovative hollow-core FRP–concrete–steel bridge columns.* Journal of Bridge Engineering, 2016: p. 04016120.
10. Abdelkarim, O.I., et al., *Hollow-Core FRP-Concrete-Steel Bridge Columns Under Extreme Loading*. 2015.
11. Abdelkarim, O.I., et al. *Seismic behavior of hollow-core FRP-concrete-steel bridge columns*. Structures Congress 2015.